Majorana Bound States in the Presence of Half-Smeared Potential

S. Basak and A. Ptok

Institute of Nuclear Physics, Polish Academy of Sciences, W.E. Radzikowskiego 152, PL-31342 Kraków, Poland

Doi: 10.12693/APhysPolA.143.164 *e-mail: surajit.basak@ifj.edu.pl

The Majorana bound state can be realized in one-dimensional chain, in form of two well-localized and separated states at both ends of the chain. In this paper, we discuss the case when the potential is smeared at one end of the system. In our investigation, we assume the smearing in the form of a quadratic function of position. We show that the smearing potential leads to the emergence of extra in-gap states, and effectively decreases the local gap (around the smeared potential). The Majorana states are still preserved in the system, however, their localization depends on the smearing. Moreover, the symmetric localization of the Majorana states from both sides of the system is no longer preserved in the presence of the smearing potential.

topics: Majorana bound states, nanowire, topological system

1. Introduction

The idea of the realization of the Majorana quasiparticles at the ends of a chain, introduced by Alexei Kitaev [1], iniciated a period of intensive studies on this issue [2–6]. Recently, several setups to realize the Majorana bound states (MBS) have been explored — e.g. monoatomic magnetic chain deposited on a superconducting surface [7–15] or hybrid superconductor/semiconductor devices [16–23].

The realization of MBS is an attractive topic due to its predicted application in constructing topologically protected Majorana-based qubits [24]. Decoherence-free quantum computing operation is related to the ability to store information nonlocaly [25]. In the standard picture, this protection is guaranteed by a high degree of spatial nonlocality of MBS. Although localized in space themselves, the Majorana quasiparticle, together with its pair, behaves like a single fermion, nonlocal in space. By a highly nonlocal MBS, we mean that MBS at the ends of the wire have almost zero overlap with each other. The degree of Majorana nonlocality η^2 can be understood as a quantity denoting the overlapping of the MBS wave functions [26]. Highly nonlocal MBS are characterized by $\eta \to 0$ (absence of overlapping), while $\eta \to 1$ (maximal overlapping) indicates that MBS are not so well localized at the boundaries. On the other hand, the overlapping of the wave function is related to the observed MBS energy. Experimentally, Majorana nonlocality can be measured from the splitting due to the hybridization of zero modes in resonance with the quantum dot state at one end of the nanowire [27].

Now, we briefly describe a typical hybrid superconductor/semiconductor device studied experimentally. The device is based on semiconducting nanowires with an epitaxial superconductor layer on three facets of the wire, grown by molecular beam epitaxy [28]. Such a prepared system is characterized by a hard-induced superconducting gap [29]. Electrostatic control of wire and barrier density is provided by side gates and a global back gate. A quantum dot (QD) can also be realized in this setup at the bare end (not covered by a superconductor) of the semiconducting wire [23]. The QD occupancy is tuned by the voltage on the gates close to the dot region. In a natural way, the spatial profile of the gate voltage leads to a non-homogeneous carrier distribution [30]. In this paper, we will discuss, how the smearing of the potential at one end of the nanowire affects the properties of MBS.

Modification of the potential along the system can be expected in several situations. For example, in presence of gate potentials (mentioned in the previous paragraph) or in the case of topological superfluid in an optical trap. In the first case, attaching the wire to a two-dimensional plaquette allows the emergence of a pair of zero-energy edge states (one localized at the end of the wire and the second one localized at the edge of plaquette) [31]. However, the experimental realization of such a system indicates the formation of the zero-mode from coalescing Andreev bound states [32]. In the second case, the shape of the optical trap potential strongly affects the realized topological phase [33–37]. To summarize, the local potential in the system has a huge impact on the MBS properties [38–40] and can lead

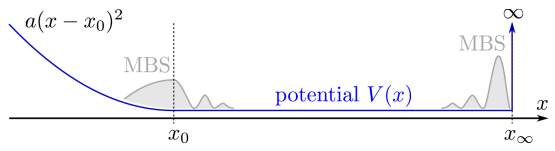

Fig. 1. Schematic representation of the discussed system with half-smeared potential $V(x)$ (blue line). The Majorana bound states (MBS) are induced at the end of the system. The localization of MBS strongly depends on the shape of $V(x)$.

to the modification of the MBS localization. Finally, it is worth mentioning that the inhomogeneity introduced due to the local potential [41–51], or the attachment of QD to the nanowire [30, 52–54] can lead to the emergence of additional in-gap states.

In the context of the arguments mentioned above, it is fair to ask how the smearing of the local potential at one end of the nanowire affects the properties of MBS. This paper is organized as follows. First, we briefly describe the used model and technique (Sect. 2). Next, in Sect. 3, we present and discuss our numerical results, which are concluded in Sect. 4.

2. Theoretical background

In this paper, we discuss the half-smeared potential presented in Fig. 1. From the right side of the nanowire, we assume a sharp step of the potential $V(x) \to \infty$, while from the left side — parabolic-like potential $V(x) \sim (x - x_0)^2$. In the central part of the system, we assume a homogeneous potential

$$V(x) = \begin{cases} a(x-x_0)^2, & \text{for} \quad x < x_0, \\ 0, & \text{for} \quad x_0 \le x \le x_\infty, \\ +\infty, & \text{for} \quad x_\infty < x, \end{cases} \tag{1}$$

Here, a is a free parameter to control smearing. In the general case, a has the unit eV/Å^2. However, in our case, x is dimensionless, while a has the dimension of energy.

We describe our system by the following Hamiltonian

$$\mathcal{H} = \mathcal{H}_0 + \mathcal{H}_{SO} + \mathcal{H}_{SC} + \mathcal{H}_V. \tag{2}$$

Here, $\mathcal{H}_0 = \sum_{i,j\sigma}[-t\,\delta_{\langle i,j\rangle} - (\mu + \sigma h)\,\delta_{ij}]\,c^\dagger_{i\sigma}c_{j\sigma}$ denotes the kinetic term, which describes the hopping of electrons between nearest-neighbor sites; $c_{i\sigma}$ ($c^\dagger_{i\sigma}$) denotes the annihilation (creation) operator of an electron with spin σ at site i; t is the hopping integral; μ is the chemical potential; and h is a Zeeman magnetic field. We neglect the orbital (diamagnetic) pair-breaking effects [55]. The spin–orbit coupling is descrbied by $\mathcal{H}_{SO} = -\mathrm{i}\lambda\sum_{i\sigma\sigma'} c_{i\sigma}(\hat{\sigma}_y)_{\sigma\sigma'}c_{i+1\sigma'} + \text{h.c.}$, where $\hat{\sigma}_y$ is the Pauli y-matrix. Superconductivity is described by the BCS-like term $\mathcal{H}_{SC} = \sum_i(\Delta\, c_{i\downarrow}c_{i\uparrow} + \text{h.c.})$, where Δ denotes superconducting gap. Finally, we introduce the half-smeared potential $\mathcal{H}_V = \sum_{i\sigma} V(i)c^\dagger_{i\sigma}c_{i\sigma}$, where we assume $V(x)$ in the form (1), where $x \equiv |\boldsymbol{R}_i|$ denotes the position of the i site. This system is presented schematically in Fig. 1. Here, the free parameter a can be treated as a parameter that controls the smearing of the potential $V(x)$. For $1/a \to 0$ we get exactly a 1D chain, while for $a \to 0$, we have a half-open chain.

In the presence of $V(x)$, the system is highly non-homogeneous. Thus, the quasiparticle spectrum of $\mathcal{H}$ can be obtained from the diagonalization procedure based on the Bogoliubov–Valatin transformation

$$c_{i\sigma} = \sum_n \left(u_{in\sigma}\gamma_n - \sigma v^*_{in\sigma}\gamma^\dagger_n\right), \tag{3}$$

where γ_n and $\gamma^\dagger_n$ are the "new" quasiparticle fermionic operators. The coefficients $u_{in\sigma}$ and $v_{in\sigma}$ satisfy the Bogoliubov–de Gennes (BdG) equations $\mathcal{E}_n\,\Psi_{in} = \sum_j \mathbb{H}_{ij}\,\Psi_{jn}$ [56], where $\Psi_{in} = (u_{in\uparrow}, u_{in\downarrow}, v_{in\downarrow}, v_{in\uparrow})$ is a four-component spinor, while the matrix $\mathbb{H}$ is defined as

$$\mathbb{H}_{ij} = \begin{pmatrix} H_{ij\uparrow\uparrow} & H_{ij\uparrow\downarrow} & \Delta_{ij} & 0 \\ H_{ij\downarrow\uparrow} & H_{ij\downarrow\downarrow} & 0 & \Delta_{ij} \\ \Delta^*_{ij} & 0 & -H^*_{ij\downarrow\downarrow} & H^*_{ij\downarrow\uparrow} \\ 0 & \Delta^*_{ij} & H^*_{ij\uparrow\downarrow} & -H^*_{ij\uparrow\uparrow} \end{pmatrix}, \tag{4}$$

where $H_{ij\sigma\sigma'} = [-t\,\delta_{\langle i,j\rangle} - (\bar{\mu}_i + \sigma h)\,\delta_{ij}]\delta_{\sigma\sigma'} + H^{\sigma\sigma'}_{SO}$ and $\Delta_{ij} = \Delta\delta_{ij}$. Here $\bar{\mu}_i = \mu - V(i)$ is an *effective* local on-site chemical potential. We introduce the following spin–orbit terms: $H^{\uparrow\downarrow}_{SO} = \lambda(\delta_{i+1,j} - \delta_{i-1,j})$, $H^{\uparrow\uparrow}_{SO} = H^{\downarrow\downarrow}_{SO} = 0$ and $H^{\downarrow\uparrow}_{SO} = (H^{\uparrow\downarrow}_{SO})^*$.

3. Numerical results

In our calculation, we considered a one-dimensional system with 1000 sites, while the part with homogeneous potential has $x_\infty - x_0 = 100$ sites (see (1)) — this length of homogeneous potential is sufficient to realize the zero-energy MBS.

Let us start by analyzing the spectrum as a function of the magnetic field in case of a sharp and maximally smeared potential (Fig. 2). In the sharp potential case ($a \to \infty$), our system is identical to the finite nanowire (Fig. 2a). The transition from the trivial phase to the topological phase occurs at some critical magnetic field $h_c = \sqrt{\Delta^2 + \tilde{\mu}^2}$ [57–59], where $\tilde{\mu} = \mu + 2t$ is the chemical potential measured from the bottom of the band. Indeed, for the discussed set of parameters, at $h = h_c \simeq \Delta$ the trivial gap is closed and a new topological gap is reopened (see Fig. 2). For $h > h_c$ the in-gap zero-energy MBS are observed, while for a relatively large h we observe typical oscillation of the in-gap states around the zero-energy level. Nevertheless, for small h, MBS have zero energies and are well localized at the boundaries of the system.

In the case of the maximally smeared potential (i.e., $a \simeq 25 \times 10^{-7}$), the main features of the spectrum is preserved (cf. panels (a) and (b) in Fig. 2). However, the additional local on-site potential leads to a situation when more sites are occupied — this

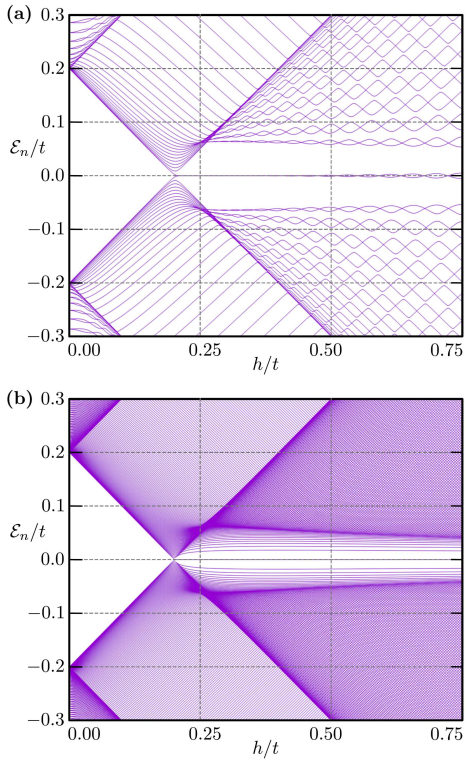

Fig. 2. Eigenstates of the system for different smearing, controlled by the a value. Panel (a) presents results for the nanowire with wall potential (large a), and (b) for the nanowire with maximally smeared potential (small a). Results obtained for $\Delta/t = 0.2$, $\mu/t = -2$, and $\lambda/t = 0.1$.

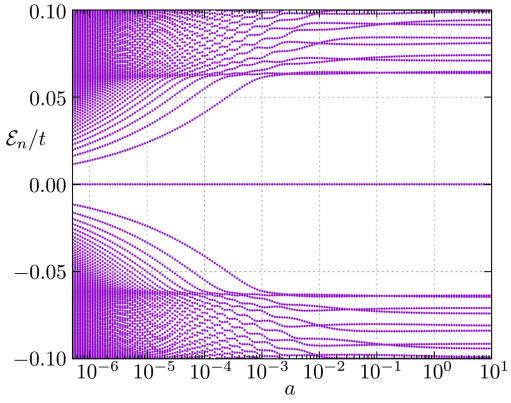

Fig. 3. Evolution of the system eigenstates with smearing parameter a. Results obtained for $h/t = 0.3$, $\mu/t = -2$, and $\Delta/t = 0.2$.

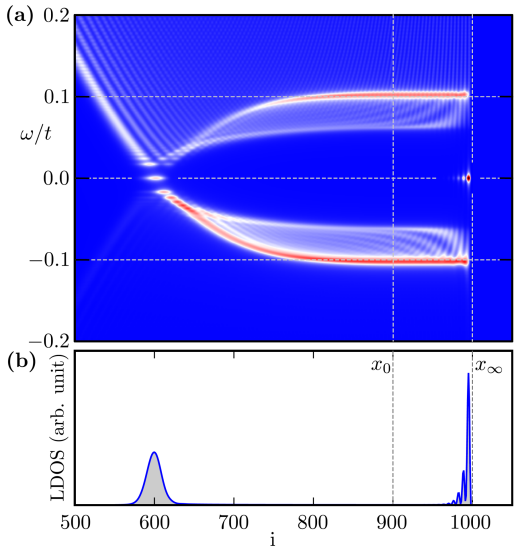

Fig. 4. (a) The local density of states (LDOS) along the system and (b) its profile for $\omega/t = 0$. Results obtained for $h/t = 0.3$, $\mu/t = -2$, $\Delta/t = 0.2$, and $a = 10^{-6}$.

is reflected in the increased number of states observed in the presented range of energies. Again, zero-energy MBS are observed, while (for $h > h_c$) more in-gap states are realized in the initial topological gap (Fig 2b). These extra in-gap states are related to states localized at the end of the system with the smeared potential (and will be discussed later).

The above-mentioned features are directly related to the smearing of the potential, and can be observed in Fig. 3, where we present the spectrum of the system as a function of a, for a fixed $h/t = 0.3$. Even for a relatively large $a \simeq 10^{-1}$, the modification of the eigenvalues of the system is clearly visible for states outside the initial topological gap (which for chosen sets of parameters are given in the range $|\mathcal{E}_n|/t < 0.65$). However, around $a \simeq 10^{-3}$, the potential induces some extra states within the topological gap. The number of these extra in-gap states increases with decreasing a. In practice, this feature can be explained as the consequence of two events. First, the smeared potential effectively increases the number of occupied sites (for the sharp potential, i.e., precisely nanowire geometry, the number of sites was 100, while for the maximally smearing potential, this number increases effectively to 400). Second, as a result of increased smearing ($a \to 0$), a bigger part of the system full-fill the condition for the realization of the topological phase. Modification of the local on-site potential μ_i by the smearing part $V(x)$ effectively leads to a local reduction of the gap.

The extra in-gap states localization and the local gap suppression can be analyzed using the local density of states (LDOS), which can be found directly from the solution of the BdG equations as [60]

$$\rho(i,\omega) = \sum_{n,\sigma} \Big[|u_{in\sigma}|^2 \delta\left(\omega - \mathcal{E}_n\right) + |v_{in\sigma}|^2 \delta\left(\omega + \mathcal{E}_n\right) \Big], \tag{5}$$

where $\delta(\omega)$ is the Dirac delta function, while $u_{in\sigma}$, $v_{in\sigma}$, and $\mathcal{E}_n$ are determined from the BdG equations. The results of the LDOS calculation are presented in Fig. 4a, where on the right side (x_∞) we set the sharp wall potential, and the smearing

potential is realized on the left site from x_0. The smearing of the potential leads to an effective decrease of the local gap, which is visible in LDOS in the form of a shears-like structure. Occupied states are realized for $x > 600$, while MBS are visible as two peaks at zero energy. The extra in-gap states are mostly localized in the left part of the system (along the smeared potential). A similar situation was observed in the case of trapped fermionic superfluids [37], where the trap potential led to an effective decrease of the gap.

Nevertheless, the gap is still open and MBS exist in the system. However, in the presence of smearing potential from one site of the system, the localization of MBS shows different features. In Fig. 4b, we present the LDOS profile for zero-energy states. In the case of a homogeneous system, MBS are characterized by oscillating wave functions. Indeed, the behavior is preserved for the state around x_∞, where the oscillating character is clearly visible. In contrast to this, the localization of the second MBS is described by a bell shaped curve (around $x = 600$). Additionally, the oscillating character is no longer observed.

4. Conclusions

To summarize, in this paper we discuss the main features of Majorana bound states in the system with a half-smeared potential. In our investigation, we assume the potential to be a quadratic function of position. We show that the smearing potential leads to the emergence of few extra in-gap states and effective decrease of the local gap. The new in-gap states are well localized around the smearing potential. However, changing the on-site potential by smearing also modifies the distribution of the particles in the system. Around the last occupied sites (around the smearing potential) the effective gap decreases. However, the gap is still open and the Majorana states are realized in the system. Nevertheless, the smeared potential affects the localizations of Majorana states, while states no longer have symmetric localization. One of the Majorana states preserves its oscillating character in space, while the second one localizes in the form of a bell-shaped curve.

Acknowledgments

S.B. is grateful to IT4Innovations (VŠB-TU Ostrava) for hospitality during a part of the work on this project. This work was supported by the National Science Centre (NCN, Poland) under grants No. 2017/25/B/ST3/02586 (S.B.) and 2021/43/B/ST3/02166 (A.P.). A.P. appreciates funding in the frame of scholarships of the Minister of Science and Higher Education (Poland) for outstanding young scientists (2019 edition, no. 818/STYP/14/2019).

References

[1] A.Y. Kitaev, *Phys.-Usp.* **44**, 131 (2001).

[2] M. Leijnse, K. Flensberg, *Semicond. Sci. Technol.* **27**, 124003 (2012).

[3] C. Bena, *C. R. Phys.* **18**, 349 (2017).

[4] R. Aguado, *Riv. Nuovo Cimento* **40**, 523 (2017).

[5] R.M. Lutchyn, E.P.A.M. Bakkers, L.P. Kouwenhoven, P. Krogstrup, C.M. Marcus, Y. Oreg, *Nat. Rev. Mater.* **3**, 52 (2018).

[6] R. Pawlak, S. Hoffman, J. Klinovaja, D. Loss, E. Meyer, *Prog. Part. Nucl. Phys.* **107**, 1 (2019).

[7] S. Nadj-Perge, I.K. Drozdov, J. Li, H. Chen, S. Jeon, J. Seo, A.H. MacDonald, B.A. Bernevig, A. Yazdani, *Science* **346**, 602 (2014).

[8] R. Pawlak, M. Kisiel, J. Klinovaja, T. Meier, S. Kawai, T. Glatzel, D. Loss, E. Meyer, *npj Quantum Inf.* **2**, 16035 (2016).

[9] M. Ruby, B.W. Heinrich, Y. Peng, F. von Oppen, K.J. Franke, *Nano Lett.* **17**, 4473 (2017).

[10] S. Jeon, Y. Xie, J. Li, Z. Wang, B.A. Bernevig, A. Yazdani, *Science* **358**, 772 (2017).

[11] B.E. Feldman, M.T. Randeria, J. Li, S. Jeon, Y. Xie, Z. Wang, I.K. Drozdov, B.A. Bernevig, A. Yazdani, *Nat. Phys.* **13**, 286 (2017).

[12] M. Steinbrecher, R. Rausch, K.T. That, J. Hermenau, A.A. Khajetoorians, M. Potthoff, R. Wiesendanger, J. Wiebe, *Nat. Commun.* **9**, 2853 (2018).

[13] A. Kamlapure, L. Cornils, J. Wiebe, R. Wiesendanger, *Nat. Commun.* **9**, 3253 (2018).

[14] H. Kim, A. Palacio-Morales, T. Posske, L. Rózsa, K. Palotás, L. Szunyogh, M. Thorwart, R. Wiesendanger, *Sci. Adv.* **4**, eaar5251 (2018).

[15] L. Schneider, S. Brinker, M. Steinbrecher, J. Hermenau, T. Posske, M. dos Santos Dias, S. Lounis, R. Wiesendanger, J. Wiebe, *Nat. Commun.* **11**, 4707 (2020).

[16] V. Mourik, K. Zuo, S.M. Frolov, S.R. Plissard, E.P.A.M. Bakkers, L.P. Kouwenhoven, *Science* **336**, 1003 (2012).

[17] A. Das, Y. Ronen, Y. Most, Y. Oreg, M. Heiblum, H. Shtrikman, *Nat. Phys.* **8**, 887 (2012).

[18] M.T. Deng, C.L. Yu, G.Y. Huang, M. Larsson, P. Caroff, H.Q. Xu, *Nano Lett.* **12**, 6414 (2012).

[19] S.M. Albrecht, A.P. Higginbotham, M. Madsen, F. Kuemmeth, T.S. Jespersen, J. Nygård, P. Krogstrup, C.M. Marcus, *Nature* **531**, 206 (2016).

[20] M.T. Deng, S. Vaitieknas, E.B. Hansen, J. Danon, M. Leijnse, K. Flensberg, J. Nygård, P. Krogstrup, C.M. Marcus, *Science* **354**, 1557 (2016).

[21] Ö. Gül, H. Zhang, F.K. de Vries et al., *Nano Lett.* **17**, 2690 (2017).

[22] J. Chen, P. Yu, J. Stenger, M. Hocevar, D. Car, S.R. Plissard, E.P.A.M. Bakkers, T.D. Stanescu, S.M. Frolov, *Sci. Adv.* **3**, e1701476 (2017).

[23] J. Chen, B.D. Woods, P. Yu, M. Hocevar, D. Car, S.R. Plissard, E.P.A.M. Bakkers, T.D. Stanescu, S.M. Frolov, *Phys. Rev. Lett.* **123**, 107703 (2019).

[24] D. Aasen, M. Hell, R.V. Mishmash et al., *Phys. Rev. X* **6**, 031016 (2016).

[25] C. Nayak, S.H. Simon, A. Stern, M. Freedman, S. Das Sarma, *Rev. Mod. Phys.* **80**, 1083 (2008).

[26] F. Peñaranda, R. Aguado, P. San-Jose, Elsa Prada, *Phys. Rev. B* **98**, 235406 (2018).

[27] M.-T. Deng, S. Vaitiekėnas, E. Prada, P. San-Jose, J. Nygård, P. Krogstrup, R. Aguado, C.M. Marcus, *Phys. Rev. B* **98**, 085125 (2018).

[28] P. Krogstrup, N.L.B. Ziino, W. Chang, S.M. Albrecht, M.H. Madsen, E. Johnson, J. Nygård, C.M. Marcus, T.S. Jespersen, *Nat. Mater.* **14**, 400 (2015).

[29] W. Chang, S. M. Albrecht, T. S. Jespersen, F. Kuemmeth, P. Krogstrup, J. Nygård, C.M. Marcus, *Nat. Nanotech.* **10**, 232 (2015).

[30] A. Kobiałka, A. Ptok, *J. Phys. Condens. Matter* **31**, 185302 (2019).

[31] A. Kobiałka, T. Domański, A. Ptok, *Sci. Rep.* **9**, 12933 (2019).

[32] H.J. Suominen, M. Kjaergaard, A.R. Hamilton, J. Shabani, C.J. Palmstrøm, C.M. Marcus, F. Nichele, *Phys. Rev. Lett.* **119**, 176805 (2017).

[33] X.-J. Liu, H. Hu, *Phys. Rev. A* **85**, 033622 (2012).

[34] X.-J. Liu, P.D. Drummond, *Phys. Rev. A* **86**, 035602 (2012).

[35] Y. Xu, L. Mao, B. Wu, C. Zhang, *Phys. Rev. Lett.* **113**, 130404 (2014).

[36] X.-J. Liu, *Phys. Rev. A* **91**, 023610 (2015).

[37] A. Ptok, A. Cichy, T. Domański, *J. Phys. Condens. Matter* **30**, 355602 (2018).

[38] C. Fleckenstein, F. Domnguez, N. Traverso Ziani, B. Trauzettel, *Phys. Rev. B* **97**, 155425 (2018).

[39] C. Moore, C. Zeng, T.D. Stanescu, S. Tewari, *Phys. Rev. B* **98**, 155314 (2018).

[40] Z. Cao, H. Zhang, H.-F. Lü, W.-X. He, H.-Z. Lu, X.C. Xie, *Phys. Rev. Lett.* **122**, 147701 (2019).

[41] D. Rainis, L. Trifunovic, J. Klinovaja, D. Loss, *Phys. Rev. B* **87**, 024515 (2013).

[42] J. Cayao, E. Prada, P. San-Jose, R. Aguado, *Phys. Rev. B* **91**, 024514 (2015).

[43] C.-X. Liu, J.D. Sau, T.D. Stanescu, S. Das Sarma, *Phys. Rev. B* **96**, 075161 (2017).

[44] Y. Huang, H. Pan, C.-X. Liu, J.D. Sau, T.D. Stanescu, S. Das Sarma, *Phys. Rev. B* **98**, 144511 (2018).

[45] C. Moore, T.D. Stanescu, S. Tewari, *Phys. Rev. B* **97**, 165302 (2018).

[46] C. Reeg, O. Dmytruk, D. Chevallier, D. Loss, J. Klinovaja, *Phys. Rev. B* **98**, 245407 (2018).

[47] T.D. Stanescu, S. Tewari, *Phys. Rev. B* **100**, 155429 (2019).

[48] O.A. Awoga, J. Cayao, A.M. Black-Schaffer, *Phys. Rev. Lett.* **123**, 117001 (2019).

[49] H. Pan, S. Das Sarma, *Phys. Rev. Res.* **2**, 013377 (2020).

[50] P. Marra, A. Nigro, *J. Phys. Condens. Matter* **34**, 124001 (2022).

[51] O.A. Awoga, J. Cayao, A.M. Black-Schaffer, *Phys. Rev. B* **105**, 144509 (2022).

[52] A. Ptok, A. Kobia lka, T. Domański, *Phys. Rev. B* **96**, 195430 (2017).

[53] E. Prada, R. Aguado, P. San-Jose, *Phys. Rev. B* **96**, 085418 (2017).

[54] D. Chevallier, P. Szumniak, S. Hoffman, D. Loss, J. Klinovaja, *Phys. Rev. B* **97**, 045404 (2018).

[55] B. Kiczek, A. Ptok, *J. Phys. Condens. Matter* **29**, 495301 (2017).

[56] P.G. de Gennes, *Superconductivity of Metals and Alloys*, Addison-Wesley, 1989.

[57] M. Sato, Y. Takahashi, S. Fujimoto, *Phys. Rev. Lett.* **103**, 020401 (2009).

[58] M. Sato, S. Fujimoto, *Phys. Rev. B* **79**, 094504 (2009).

[59] M. Sato, Y. Takahashi, S. Fujimoto, *Phys. Rev. B* **82**, 134521 (2010).

[60] H. Matsui, T. Sato, T. Takahashi, S.-C. Wang, H.-B. Yang, H. Ding, T. Fujii, T. Watanabe, A. Matsuda, *Phys. Rev. Lett.* **90**, 217002 (2003).